



## Structural, Magnetic and Adsorption Characteristics of Magnetite Nanoparticles Prepared from Spent Pickle Liquor

Shaimaa T. El-Wakeel, Emad K. Radwan, Amer S. El-Kalliny\*, Tarek A. Gad-Allah, and Iman Y. El-Sherif.

Department of Water Pollution Research, National Research Centre, 33 EL Bohouthst. (former EL Tahrirst.), Dokki, Giza Egypt-P. O. 12622.

**Abstract :** From the spent pickle liquor, magnetite nanoparticles ( $\text{Fe}_3\text{O}_4\text{NPs}$ ) with high crystallinity and high saturation magnetization were prepared by hydrothermal process. The characteristics of the materials, prepared via different hydrothermal time durations, were investigated by X-ray diffraction (XRD), high-resolution transmission electron microscope (HR-TEM), Energy-dispersive X-ray (EDX), and vibrating sample magnetometry (VSM) techniques. The adsorption behavior for the prepared materials towards  $\text{Pb}^{2+}$  metal ions was also studied. Moreover, equilibrium data were modeled using Freundlich, Langmuir, Temkin and Dubinin–Radushkevich equations. On the other hand, the adsorption kinetics were tested by pseudo first-order and pseudo second-order rate equations. To sum up, a well crystalline face centered cubic structure superferromagnetic  $\text{Fe}_3\text{O}_4\text{NPs}$  was obtained. The adsorption of  $\text{Pb}^{2+}$  is a pseudo second-order rate process and follows Langmuir isotherm model with a relatively high calculated maximum adsorption capacity  $[(q)_{i, \text{max}}]$ . Therefore, the prepared  $\text{Fe}_3\text{O}_4\text{NPs}$  are considered as promising magnetic adsorbents and via this research, the pickle liquor waste can be transferred into valuable magnetite materials.

**Keywords:** hydrothermal treatment; adsorption; magnetically separable materials; heavy metals; wastewater treatment.

### Introduction

Increasing heavy metals in water sources as a result of the rapid industrialization is a serious problem for the public health. Heavy metals are toxic, non-biodegradable and bioaccumulative environmental pollutants that have a global concern due to their dangerous effects on the environment<sup>1</sup>. For instance, the presence of lead in water with high concentrations causes liver and kidney damage<sup>2</sup>. Thereby, efficient removal of such pollutants from water and wastewater became mandatory to avoid their negative impacts.

Recently magnetic nanoparticles (NPs), magnetite ( $\text{Fe}_3\text{O}_4$ ) particularly, have been used extensively for heavy metals removal. Although simple and inexpensive procedures were developed to prepare magnetite NPs, such as co-precipitation<sup>3</sup> and sol-gel methods<sup>4</sup>, yet the need to use chemicals of reagent grade reduces their practical application. Currently, researches are focusing on the preparation of magnetite NPs from solid and/or liquid wastes<sup>5-8</sup>.

Pickle liquor is used to clean the surface of steel in various steel-making processes and electroplating industry. Its spent contains strong acids and rich with iron ions. The spent pickle liquor is considered a hazardous waste. It can be treated commonly by precipitation with lime, which produced a great amount of

residue waste. Thus, recovery of iron in spent pickle liquor is better environmentally and economically. Chen et al.<sup>9</sup> reported some new approaches for the recovery process such as electro-dialysis<sup>10</sup>, membrane distillation<sup>11</sup>, selective precipitation<sup>12</sup>, anion exchange/membrane electro-winning<sup>13</sup>, and spray roasting<sup>14</sup>. Iron salts (chlorides or sulfates), with ferrites as by-products are usually the recovered products. Few reports have been published on the synthesis of magnetite from pickle liquor. Dufour et al.,<sup>15,16</sup> prepared magnetite from sulfuric pickling waste liquor by oxidation-precipitation using ammonium hydroxide as basic agent and air as oxidizer. Ciminelli et al.,<sup>17</sup> used microwave-assisted hydrothermal method to remove metals from pickling liquors and to produce electroceramics as well. Starting with concentrated liquors, they obtained single-phase magnetite at pH = 13 and processing conditions of 110 °C and 5 min. However, they didn't discuss the characteristics of the resulting magnetite. Recently, Fang group prepared magnetite NPs from pickling waste liquor following chemical co-precipitation method under N<sub>2</sub> gas protection after adjusting the ratio of Fe<sup>2+</sup> to Fe<sup>3+</sup>. The as-prepared magnetite NPs was roughly spherical in shape with a size range of 20–50 nm. Nevertheless, the preparation process involved several steps and was somewhat expensive and complex. In one hand, they investigated the heterogeneous Fenton-like catalytic capacity of magnetite NPs for the removal of bisphenol A<sup>18</sup>. On the other hand, they functionalized the magnetite NPs with ethylenediamine in order to improve its adsorption capacity and selectivity for Cr<sup>6+</sup>. For this purpose, hydrothermal treatment is used in this work as it has many advantages: easy to control, produces highly crystallized and weakly agglomerated powders with a narrow size distribution<sup>9</sup>.

This paper reports for the first time the preparation of well crystallized magnetite NPs from real spent pickle liquor directly by a simple hydrothermal process. The produced materials via different hydrothermal time durations were fully characterized. The complete picture including the formed crystalline phases, the morphology, and the composition of the prepared adsorbents was drawn. Besides, the magnetic and the adsorption properties of the materials were determined in order to select the best preparation conditions.

## Experimental methods

### 1. Preparation of magnetic adsorbent via hydrothermal treatment

The spent pickle liquor was collected from a local iron and steel company. The main components of this waste are listed in Table 1. Heavy metal ions and sodium were determined by Inductively Coupled Plasma Optical Emission Spectrometry (ICP-OES, Agilent 5100 model). Inorganic anions were determined by Ion Chromatograph (Dionex ICS 5000, Thermo Scientific, USA).

**Table 1: Concentrations (g/L) of the main components of the used spent pickle liquor.**

Fe	Zn	Pb	Na	SO <sub>4</sub> <sup>2-</sup>	PO <sub>4</sub> <sup>2-</sup>	Cl	Br	F
62.50	25.00	1.00	1.50	4.46	15.30	323.34	9.64	0.44

The spent pickle liquor was mixed with appropriate amount of distilled water and its pH was adjusted to 11 by ammonium hydroxide solution (28–30% NH<sub>3</sub>, Sigma-Aldrich) in order to precipitate the metals hydroxides. This solution was diluted 20 times with distilled water. Then, 100 mL of the diluted waste was transferred to 125 mL Teflon-lined autoclave (Model 4748, Parr Instrument Company, USA) and heated at 200 °C for different time durations. Finally, the precipitated materials were collected and washed several times with distilled water and ethanol. Samples are labeled as M2, M24, and M72, where the number refers to the time of hydrothermal treatment.

### 2. Characterization of the prepared adsorbents

X-ray diffraction (XRD) analyses of the prepared powders at different hydrothermal treatment times were performed using BRUKER D8 ADVANCE with secondary monochromatic beam CuK $\alpha$  radiation at 40 kV and 40 mA. The microstructure and composition of the prepared adsorbents were examined under high-resolution transmission electron microscope (HR-TEM, Tecnai G20, Super twin, double tilt, FEI Co., the Netherlands) using a working voltage of 200 kV. TEM Imaging and Analysis (TIA) software was used to spectrum acquisition and analysis of Energy-dispersive X-ray (EDX) peaks. The magnetization hysteresis loops

and the magnetic properties were measured by Riken Denshi BH-55 vibrating sample magnetometer (VSM) at room temperature.

### 3. Adsorption experiments

Lead (II) nitrate (Merck) was used as sources for  $Pb^{2+}$  ions. Its concentration during the adsorption experiments was followed according to the standard methods for the examination of water and wastewater<sup>19</sup> using Atomic Absorption Spectrometer (Varian Spectra AAS 220) with graphite furnace accessory and equipped with deuterium arc background corrector. The precision of the metal ions measurement was determined by analyzing samples in triplicate and for each series of measurements an absorption calibration curve was constructed.

Adsorption experiments were carried out in a batch mode by shaking 0.5 g/L of the magnetic adsorbent with 20 mg/L of  $Pb^{2+}$  solution, without changing the solution pH, in a Pyrex glass conical. Speed of the orbital shaker (Stuart Scientific, S01, United Kingdom) was 200 rpm. All experiments were carried out at temperature of  $22 \pm 1^\circ C$ . The withdrawn samples were filtered by 0.2  $\mu m$  syringe-driven filter unit (Thermo Co.) before analysis. The amounts of  $Pb^{2+}$  adsorbed at time  $t$  ( $q_t$ , mg/g) on the magnetic adsorbents were determined by:

$$q_t = \frac{(C_0 - C_t) \cdot V}{m}, \quad (1)$$

where  $C_0$  (mg/L) is the initial concentration of  $Pb^{2+}$  ions,  $C_t$  (mg/L) is concentration of  $Pb^{2+}$  ions at definite time ( $t$ ),  $V$  (L) is the volume of the  $Pb^{2+}$  solution, and  $m$  (g) is the amount of the magnetic adsorbent.

#### 3.1. Adsorption isotherms

Isothermal studies were carried out by mixing 0.5 g/L of the prepared material with a suitable amount of  $Pb^{2+}$  solution at different initial concentrations (25 – 150mg/L) and shaking for 2 h at  $22 \pm 1^\circ C$ . Freundlich<sup>20</sup> (Eq. 2), Langmuir<sup>21</sup> (Eq. 3), Temkin<sup>22</sup> (Eq. 4) and Dubinin–Radushkevich (D-R)<sup>23</sup> (Eq. 5) models were investigated in order to determine the adsorption behavior. The linear forms of these models are as follows:

$$\log q_e = \log K_f + \frac{1}{n} \log C_e, \quad (2)$$

$$\frac{C_e}{q_e} = \frac{1}{K_L q_{max}} + \frac{C_e}{q_{max}}, \quad (3)$$

$$\frac{q_e}{b_t} = \frac{RT}{b_t} \ln a_t + RT \ln C_e, \quad (4)$$

$$\ln q_e = \ln q_{max} - \beta \varepsilon^2, \quad (5)$$

where  $q_e$  (mg/g) is the adsorption capacity at equilibrium,  $C_e$  (mg/L) is the equilibrium concentration,  $K_f$  and  $n$  are the Freundlich adsorption constants related, respectively, to the capacity and intensity of the adsorption,  $q_{max}$  (mg/g) is the maximum adsorption capacity,  $K_L$  (L/mg) is Langmuir constant;  $b_t$  (kJ/mol) is the heat of sorption constant,  $a_t$  (L/g) is the equilibrium binding constant corresponding to the maximum binding energy,  $R$  is the universal gas constant,  $T$  is the absolute temperature,  $\beta$  ( $mol^2/kJ^2$ ) is activity coefficient related to mean adsorption energy and  $\varepsilon$  is the Polanyi potential which can be calculated from:

$$\varepsilon = RT \ln \left( 1 + \frac{1}{C_e} \right) \quad (6)$$

The mean free energy ( $E$ ) of adsorption was calculated using the following equation<sup>24</sup>:

$$E = \frac{1}{\sqrt{-2\beta}} \quad (7)$$

### 3.2. Adsorption kinetics:

The adsorption kinetics process were studied through the adsorption experiments at different time intervals and constant metal concentration (20 mg/L) at  $22 \pm 1^\circ\text{C}$ . Pseudo-first-order<sup>25</sup>(Eq. 8) and pseudo-second-order<sup>26</sup>(Eq.9) models were used as follow to interpret the adsorption kinetic data:

$$\log(q_e - q_t) = \log q_e - \frac{k_1 t}{2.303}, \quad (8)$$

$$\frac{t}{q_t} = \frac{1}{k_2 q_e^2} + \frac{1}{q_e} t, \quad (9)$$

where  $q_e$  and  $q_t$  are the amounts of adsorbed metal (mg/g) at equilibrium and definite time, respectively,  $k_1$  ( $\text{min}^{-1}$ ) and  $k_2$  (g/mg.min) are the first and second rate adsorption constants, respectively.

## Results and discussion

### 1. Phase composition of the prepared materials

Crystalline structures of the prepared materials at different hydrothermal times were identified from their XRD patterns presented in Figure1. The three XRD patterns exhibit sharp and intense diffraction peaks in  $2\theta$  range of  $10 - 70^\circ$ . All of the diffraction peaks can be assigned to the inverse spinel and face centered cubic structure of  $\text{Fe}_3\text{O}_4$  according to the JCPDS card 88-0315. The average crystal domain diameter ( $D$ ) was calculated by using Debye-Scherrer equation expressed as follows:

$$D = \frac{K\lambda}{\beta \cos\theta}, \quad (10)$$

where  $K$  is a constant related to the Miller index of crystallographic planes (0.9),  $\lambda$  (nm) is the wavelength of the X-ray,  $\beta$  (radians) is the angular width at half-maximum intensity, and  $\theta$  is half of the diffraction angle<sup>27</sup>. The crystal sizes of the synthesized  $\text{Fe}_3\text{O}_4$ NPs were calculated at the most intense peak ( $2\theta = 35.4^\circ$ ). As the time of the hydrothermal treatment increase from 2 h to 24 h and finally to 72 h, the  $\text{Fe}_3\text{O}_4$  crystals grew from 12 nm, to 16 nm and finally to 30 nm and consequently the enhancement of  $\text{Fe}_3\text{O}_4$  peaks was observed.

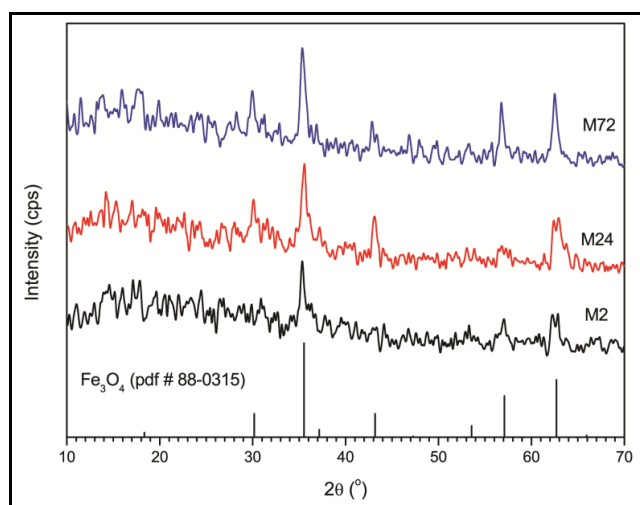


Figure1: XRD patterns of the prepared  $\text{Fe}_3\text{O}_4$  samples.

## 2. Microstructure of the prepared materials

The TEM image of the prepared material M2 in Figure2a show anhedral structure of NPs. Upon increase in hydrothermal treatment time to 24 h (M24, Figure2b), two different morphologies appeared clearly. Some particles appeared to be roughly polyhedron in shape and some exist in flakes-like shape. The polyhedron particles become predominant at hydrothermal treatment time of 72 h (M72, Figure2c) with appearance of rods-like particles instead of flakes-like particles. Selected area electron diffraction (SAED) analysis (Inset in Figure2c) confirmed that the rods-like particles have not clear diffraction planes (i.e., no ring patterns was observed) leading to the fact that these particles are amorphous in nature. These amorphous particles are considered as impurities, which increase the noise in XRD patterns. On the other hand, an obvious ring-pattern was observed in the SAED analysis (Inset in Figure2c) of the polyhedral particles. This pattern demonstrates the polycrystalline nature<sup>28</sup> of the Fe<sub>3</sub>O<sub>4</sub>NPs in polyhedron morphology. The compositions of the prepared materials were investigated using EDX technique (Table 2). The materials compose mainly of Fe and O elements with traces of some elements (e.g. Pb and Zn). The calculated O/Fe ratios are in the range of 1.3 – 1.6 proving the formation of Fe<sub>3</sub>O<sub>4</sub> phase that possesses O/Fe = 1.33.

**Table 2:Elemental composition of the prepared Fe<sub>3</sub>O<sub>4</sub> NPs samples.**

Sample	OK	PbM	FeK	ZnK	O/Fe ratio
M2	60.99	0.06	37.5	1.45	1.3
M24	63.45	0.07	34.13	2.35	1.6
M72	57.44	-	39.68	-	1.4

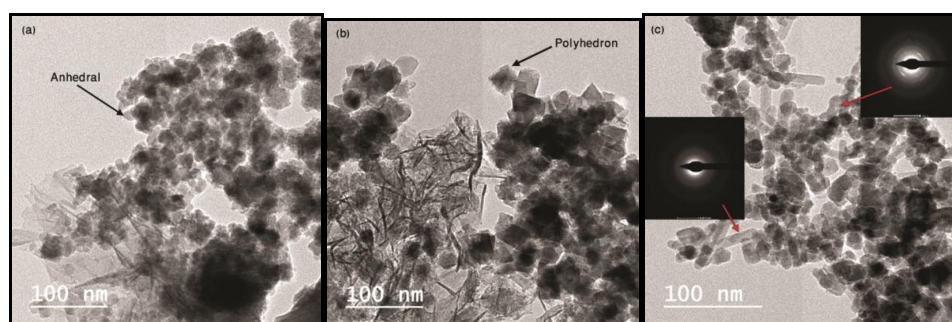


**Figure2: TEM images of (a) M2, (b) M24, and (c) M72; the insets are SAED images.**

## 3. Magnetic properties of the prepared Fe<sub>3</sub>O<sub>4</sub> NPs

It is very important to investigate the magnetic properties of the prepared Fe<sub>3</sub>O<sub>4</sub> NPs in order to assess its separation and recovery tendencies from water/wastewater after the treatment process. Figure3 represents the magnetization curves of these Fe<sub>3</sub>O<sub>4</sub>NPs and the extracted values are listed in Table 3. The small coercivity values indicate the superparamagnetic behavior for the prepared ferromagnetic adsorbents. This behavior can be attributed to the effects of small grain size composing the magnetic adsorbent<sup>29</sup>. The inset in Figure3 demonstrates the recovery of the prepared material (M24) by the action of a neodymium permanent magnet (STM-30x50-N magnet, magnets4you Co., Germany).

The saturation magnetization (M<sub>S</sub>) of M72 is little bet higher than M24. While on decreasing the time of the hydrothermal treatment to 2 h (i.e. M2 sample), the saturation magnetization markedly decreased by about 10 emu/g. This is due to the higher ratio of the crystallized polyhedron particles to the impurities of amorphous nature in samples that treated for 24 h and 72 h. The room temperature M<sub>S</sub> value of M72 is 62 emu/g which is comparable with the previously reported values<sup>30-32</sup> and lower than other reported M<sub>S</sub> values ~92 emu/g<sup>30,33,34</sup>. This could be attributed to the existence of impurities, incomplete particle crystallization, the large surface-to-volume ratio due to the small particle size<sup>31</sup>.

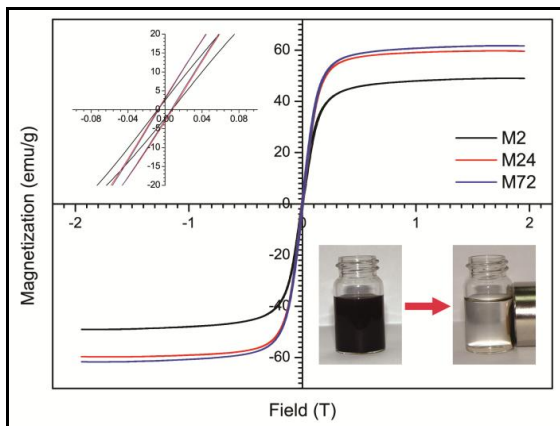


**Figure3: Magnetic hysteresis loops of the prepared Fe<sub>3</sub>O<sub>4</sub> NPs. Insets: Magnification at the origins and the photographs of magnetic separation of the prepared Fe<sub>3</sub>O<sub>4</sub> NPs.**

**Table 3: Magnetic properties of the prepared Fe<sub>3</sub>O<sub>4</sub> NPs.**

Sample	Saturation Magnetization (emu/g)	Coercivity (G)	Retentivity (emu/g)
M2	49.00	97.00	3.23
M24	60.00	101.00	4.41
M72	62.00	86.00	3.66

#### 4. Adsorption study

##### 4.1. Adsorption kinetics

Figure4 displays the adsorption of the model Pb<sup>2+</sup> metal ions on the Fe<sub>3</sub>O<sub>4</sub> NPs that prepared by hydrothermal treatment for different durations. Generally, the adsorption process is fast and reaches the equilibrium within 20 - 30 minutes. The M2 and M24 samples have similar affinities to adsorb Pb<sup>2+</sup> with peaked adsorption capacity of 36.0 and 32.8 mg/g, respectively. Upon increasing the hydrothermal treatment time to 72 h (i.e. M72 sample), the adsorption capacity was significantly decreased. Thus, 2 h is the optimum hydrothermal treatment time for the preparation of Fe<sub>3</sub>O<sub>4</sub> NPs in terms of Pb<sup>2+</sup> adsorption. Based on these results, the sample M2 was selected to explore further the adsorption kinetics and isotherms.

Knowledge about the kinetics parameters of an adsorption system is necessary to depict its efficiency. The pseudo-first-order equation describes adsorption in solid-liquid systems based on the sorption capacity of solids. On the other hand, the pseudo-second-order rate equation has been applied for analyzing chemisorption kinetics from liquid solutions. Table 4 lists the driven parameters of the pseudo-first-order and pseudo-second-order equations.

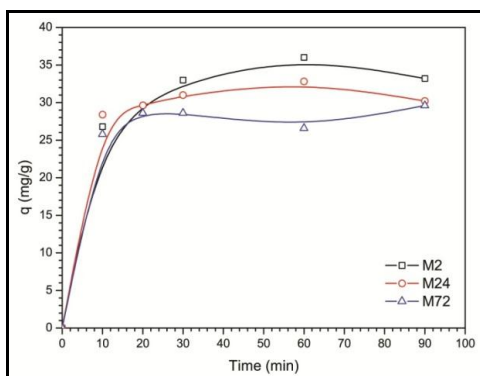


**Figure4: Adsorption behaviors of Pb<sup>2+</sup> ions on the prepared Fe<sub>3</sub>O<sub>4</sub> NPs.**



**Table 4: Driven kinetic parameters for Pb<sup>2+</sup> adsorption by M2 sample (adsorbent dose: 0.5 g/L, metal concentration: 20 mg/L, agitation speed: 200 rpm, 22 ± 1 °C).**

Pseudo-first order	$q_e \left( \frac{mg}{g} \right)$		$k_1 (min^{-1})$	$R^2$
	Experimental	Calculated		
	36	7.07	0.012	0.532
Pseudo-second order	$q_e \left( \frac{mg}{g} \right)$		$k_2 \left[ (g (mg \cdot min))^{-1} \right]$	$R^2$
	Experimental	Calculated		
	36	36.5	0.004	0.999

Table 4 shows that the  $R^2$  values were higher for pseudo-second-order equation. Moreover, the calculated  $q_e$  value agrees quite well with the experimental value. Consequently, the adsorption of Pb<sup>2+</sup> on the prepared Fe<sub>3</sub>O<sub>4</sub>NPs is best described by pseudo second-order rate process and the adsorption process might occur via a chemical reaction.

#### 4.2. Adsorption isotherms

In order to understand the adsorption mechanism and the surface properties and affinity of the adsorbent, the adsorption of Pb<sup>2+</sup> by M2 sample was modeled using Freundlich, Langmuir, Temkin and Dubinin-Radushkevich (D-R) adsorption isotherms. Table 5 lists driven parameters calculated from the plots of the linear forms of these models. According to the  $R^2$  values, it can be concluded that, although the studied models reasonably fit the equilibrium data, Langmuir model is the best fitting implying the formation of a monolayer of Pb<sup>2+</sup> onto the adsorbent surface<sup>35</sup> that has identical and equivalent number of definite sites on which adsorption occurs. The maximum adsorption capacity ( $q_{max}$ ) calculated from Langmuir isotherm model for Pb<sup>2+</sup> was compared with those of other adsorbents reported in the literature (Table 6). It can be seen that the Fe<sub>3</sub>O<sub>4</sub>NPs prepared in this study have a higher  $q_{max}$  than many reported adsorbents, indicating that Fe<sub>3</sub>O<sub>4</sub>NPs are promising adsorbents for Pb<sup>2+</sup> removal.

The mean free-energy (E) was calculated from the data fitting according to D-R isotherm and by using Equation (7). It is argued that when the mean free energy (E) values driven from the D-R isotherm is below 8 kJ mol<sup>-1</sup>, the adsorption is a physical process and between 8 and 16 kJ mol<sup>-1</sup>, the adsorption occurs via ion exchange process<sup>36</sup>. The E value of Pb<sup>2+</sup> adsorption on M2 sample is less than 16 kJ mol<sup>-1</sup>. This indicates that the adsorption occurs via ion exchange process. Accordingly, the energy of this chemisorption was calculated from Temkin isotherm. Since, the variation of the adsorption energy is positive, the adsorption reaction is considered exothermic process<sup>37</sup>.

**Table 5: Driven isotherm parameters for Pb<sup>2+</sup> adsorption on M2 sample (adsorbent dose: 0.5 g/L, initial metal concentration: 25 – 150mg/L, contact time: 60 min, agitation speed: 200 rpm, 22 ± 1 °C).**

Langmuir isotherm parameters	$q_{max} \left( \frac{mg}{g} \right)$	$b \left( \frac{L}{mg} \right)$	$R^2$
	120.48	0.14	0.99
Freundlich isotherm parameters	$\frac{1}{n}$	$K_f \left( \frac{L}{mg} \right)$	$R^2$
	0.23	41.6	0.97
D-R isotherm parameters	$q_{max} \left( \frac{mol}{g} \right)$	$E \left( \frac{KJ}{mol} \right)$	$R^2$
	$1.16 \times 10^{-3}$	15.9	0.98
Temkin isotherm parameters	$b_t \left( \frac{J}{mol} \right)$	$a_t \left( \frac{L}{g} \right)$	$R^2$
	140.2	6.5	0.98

**Table 6: Maximum adsorption capacity ( $q_{max}$ ) of various adsorbents for  $Pb^{2+}$ .**

Adsorbent	$q_{max} \left( \frac{mg}{g} \right)$	Ref.
$Fe_3O_4$ NPs	120	This work
$Fe_3O_4$ nanosphereswith hollow interiors	19	27
Nano $Fe_3O_4/SiO_2-NH_2$	17.65	38
Activated carbon	13.05	39
Manganese oxide-coated carbon nanotubes	78.7	40
Indonesian peat	~ 80	41
Cancrinite-typeZeolite	530	42
Nanometer $TiO_2$ immobilized on silica gel	3.16	43

## Conclusion

Preparation of magnetite NPs from pickle liquor waste was carried out by hydrothermal treatment. Well crystallized face centered cubic structure of  $Fe_3O_4$  was obtained. HR-TEM analysis shows the increase of polyhedron NPs morphology by increasing the hydrothermal treatment time. SAED analysis confirmed that rods-like particles are amorphous in nature which are considered as impurities. It confirmed also that polyhedral particles are polycrystalline  $Fe_3O_4$  NPs. The elemental detection from EDX matched well with the  $Fe_3O_4$  composition.  $Fe_3O_4$  NPs exhibited superferromagnetic behavior which is dependent on the hydrothermal treatment time. In addition, the  $Fe_3O_4$  NPs prepared via hydrothermal treatment for 2 h showed the highest adsorption affinity towards  $Pb^{2+}$  metal ions, but from the practical point of view  $Fe_3O_4$  NPs hydrothermally treated for 24 h are the best as they are separated easily from the treated water due to its highest saturation magnetization. It was found that Langmuir isotherm model can describe the adsorption behavior of  $Pb^{2+}$  metal ions on these  $Fe_3O_4$  NPs and the calculated  $q_{max}$  was higher than many reported adsorbents. This indicates that the prepared  $Fe_3O_4$  NPs are promising adsorbents for  $Pb^{2+}$  removal and the pickle liquor waste can be transferred into valuable magnetite materials.

## Acknowledgement

The authors gratefully acknowledge the financial support provided by in House Project Office at National Research Centre, (NRC, Egypt), Project (P100808 - tenth research plane, 2015-2016).

## References

- Xu P, Zeng GM, Huang DL, et al. Use of iron oxide nanomaterials in wastewater treatment: a review. *Science of the Total Environment*. 2012;424:1-10.
- Jabeen H, Kemp KC, Chandra V. Synthesis of nano zerovalent iron nanoparticles–Graphene composite for the treatment of lead contaminated water. *Journal of environmental management*. 2013;130:429-435.
- Mel'nik I, Zub YL, Alonso B, Abramov N, Gorbik P. Creation of a functional polysiloxane layer on the surface of magnetic nanoparticles using the sol-gel method. *Glass Physics and Chemistry*. 2012;38(1):96-104.
- Wu S, Sun A, Zhai F, et al.  $Fe_3O_4$  magnetic nanoparticles synthesis from tailings by ultrasonic chemical co-precipitation. *Materials Letters*. 2011;65(12):1882-1884.
- Fang XB, Fang ZQ, Tsang PKE, Cheng W, Yan XM, Zheng LC. Selective adsorption of Cr(VI) from aqueous solution by EDA- $Fe_3O_4$  nanoparticles prepared from steel pickling waste liquor. *Applied Surface Science*. 9/30/ 2014;314:655-662.
- Sakthivel R, Vasumathi N, Sahu D, Mishra B. Synthesis of magnetite powder from iron ore tailings. *Powder Technology*. 2010;201(2):187-190.
- Kumar R, Sakthivel R, Behura R, Mishra BK, Das D. Synthesis of magnetite nanoparticles from mineral waste. *Journal of Alloys and Compounds*. 10/5/ 2015;645:398-404.



8. Giri SK, Das NN, Pradhan GC. Synthesis and characterization of magnetite nanoparticles using waste iron ore tailings for adsorptive removal of dyes from aqueous solution. *Colloids and Surfaces A: Physicochemical and Engineering Aspects*. 9/20/ 2011;389(1–3):43-49.
9. Chen D, Hou J, Yao L-h, Jin H-m, Qian G-R, Xu ZP. Ferrite materials prepared from two industrial wastes: Electroplating sludge and spent pickle liquor. *Separation and Purification Technology*. 2010;75(2):210-217.
10. Paquay E, Clarinval A-M, Delvaux At, Degrez M, Hurwitz H. Applications of electro dialysis for acid pickling wastewater treatment. *Chemical Engineering Journal*. 2000;79(3):197-201.
11. Tomaszewska M, Gryta M, Morawski A. Recovery of hydrochloric acid from metal pickling solutions by membrane distillation. *Separation and Purification Technology*. 2001;22:591-600.
12. Heras F, Dufour J, Lopez-Delgado A, Negro C, Lopez-Mateos F. Feasibility study of metals recycling from nitric-hydrofluoric waste pickle baths. *Environmental engineering science*. 2004;21(5):583-590.
13. Csicsovszki G, Kékesi T, Török TI. Selective recovery of Zn and Fe from spent pickling solutions by the combination of anion exchange and membrane electrowinning techniques. *Hydrometallurgy*. 2005;77(1):19-28.
14. Kladnig WF. A review of steel pickling and acid regeneration an environmental contribution. *International Journal of Materials and Product Technology*. 2003;19(6):550-561.
15. Dufour J, López L, Negro C, Latorre R, Formoso A, Lopez-Mateos F. Mathematical model of magnetite synthesis by oxidation of sulfuric pickling liquors from steelmaking. *Chemical Engineering Communications*. 2002;189(3):285-297.
16. Dufour J, Marrón J, Negro C, Latorre R, Formoso A, López-Mateos F. Mechanism and kinetic control of the oxy precipitation of sulphuric liquors from steel pickling. *Chemical Engineering Journal*. 1997;68(2):173-187.
17. Ciminelli VST, Dias A, Braga HC. Simultaneous production of impurity-free water and magnetite from steel pickling liquors by microwave-hydrothermal processing. *Hydrometallurgy*. 2006;84(1):37-42.
18. Huang R, Fang Z, Fang X, Tsang EP. Ultrasonic Fenton-like catalytic degradation of bisphenol A by ferrous oxide ( $\text{Fe}_3\text{O}_4$ ) nanoparticles prepared from steel pickling waste liquor. *Journal of colloid and interface science*. 2014;436:258-266.
19. Rice E, Baird R, Eaton A, Clesceri L. *Standard methods for the examination of water and wastewater*: American Public Health Association, Washington, DC; 2012.
20. Freundlich HMF. Over the adsorption in solution. *Journal of Physical Chemistry*. 1906; 57: 385-470.
21. Langmuir I. The adsorption of gases on plane surfaces of glass, mica and platinum. *J Am Chem Soc*. Jul-Dec 1918;40:1361-1403.
22. Temkin MI, Pyzhev V. Kinetics of ammonia synthesis on promoted iron catalyst. *Acta Physiochim* 1940;URSS 12:327-356.
23. Dubinin MM, Radushkevich LV. The equation of the characteristic curve of the activated charcoal. *Proc. Acad. Sci. USSR Phys. Chem. Sect.* . 1947;55:331-337.
24. Erdem E, Karapinar N, Donat R. The removal of heavy metal cations by natural zeolites. *Journal of colloid and interface science*. 2004;280(2):309-314.
25. Yuh-Shan H. Citation review of Lagergren kinetic rate equation on adsorption reactions. *Scientometrics*. 2004;59(1):171-177.
26. Ho Y-S. Review of second-order models for adsorption systems. *Journal of hazardous materials*. 2006;136(3):681-689.
27. Kumari M, Pittman CU, Mohan D. Heavy metals [chromium (VI) and lead (II)] removal from water using mesoporous magnetite ( $\text{Fe}_3\text{O}_4$ ) nanospheres. *Journal of colloid and interface science*. 2015;442:120-132.
28. Shen X, Garces L-J, Ding Y, et al. Behavior of  $\text{H}_2$  chemisorption on Ru/ $\text{TiO}_2$  surface and its application in evaluation of Ru particle sizes compared with TEM and XRD analyses. *Applied Catalysis A: General*. 2008;335(2):187-195.
29. Huang X, Zhang J, Xiao S, Sang T, Chen G. Unique electromagnetic properties of the zinc ferrite nanofiber. *Materials Letters*. 2014;124:126-128.
30. Peternele WS, Fuentes VM, Fascineli ML, et al. Experimental investigation of the coprecipitation method: An approach to obtain magnetite and maghemite nanoparticles with improved properties. *Journal of Nanomaterials*. 2014;2014:94.

31. Rajput S, Pittman CU, Mohan D. Magnetic Magnetite (Fe<sub>3</sub>O<sub>4</sub>) Nanoparticle Synthesis and Applications for Lead (Pb<sup>2+</sup>) and Chromium (Cr<sup>6+</sup>) Removal from Water. *Journal of Colloid and Interface Science*. 2015.
32. Salazar-Camacho C, Villalobos M, de la Luz Rivas-Sánchez M, Arenas-Alatorre J, Alcaraz-Cienfuegos J, Gutiérrez-Ruiz ME. Characterization and surface reactivity of natural and synthetic magnetites. *Chemical Geology*. 2013;347:233-245.
33. Roca AG, Marco JF, Morales MdP, Serna CJ. Effect of nature and particle size on properties of uniform magnetite and maghemite nanoparticles. *The Journal of Physical Chemistry C*. 2007;111(50):18577-18584.
34. Wang B, Wei Q, Qu S. Synthesis and characterization of uniform and crystalline magnetite nanoparticles via oxidation-precipitation and modified co-precipitation methods. *Int J Electrochem Sci*. 2013;8:3786-3793.
35. Tang XH, Zhang XM, Guo CC, Zhou AL. Adsorption of Pb<sup>2+</sup> on Chitosan Cross-Linked with Triethylene-Tetramine. *Chemical engineering & technology*. 2007;30(7):955-961.
36. CI E, Umedum N, Anarado C, Eboatu A. Chicken Feather as Sequestrant for Lead Ions in Aqueous Solution. *Int. J. Modern Anal. Sep. Sci*. 2014;3(1):51-66.
37. Mohammed AA-A. Thermodynamics approach in the adsorption of heavy metals. In: Pirajã;n JCM, ed. *Thermodynamics - Interaction Studies - Solids, Liquids and Gases.*: InTech; 2011.
38. Mahdavi M, Ahmad MB, Haron MJ, Gharayebi Y, Shameli K, Nadi B. Fabrication and Characterization of SiO<sub>2</sub>/(3-Aminopropyl)triethoxysilane-Coated Magnetite Nanoparticles for Lead(II) Removal from Aqueous Solution. *Journal of Inorganic and Organometallic Polymers and Materials*. 2013;23(3):599-607.
39. Imamoglu M, Tekir O. Removal of copper (II) and lead (II) ions from aqueous solutions by adsorption on activated carbon from a new precursor hazelnut husks. *Desalination*. 2008/08/15 2008;228(1):108-113.
40. Wang S-G, Gong W-X, Liu X-W, Yao Y-W, Gao B-Y, Yue Q-Y. Removal of lead(II) from aqueous solution by adsorption onto manganese oxide-coated carbon nanotubes. *Separation and Purification Technology*. 12/1/ 2007;58(1):17-23.
41. Balasubramanian R, Perumal S, Vijayaraghavan K. Equilibrium isotherm studies for the multicomponent adsorption of lead, zinc, and cadmium onto Indonesian peat. *Industrial & Engineering Chemistry Research*. 2009;48(4):2093-2099.
42. Qiu W, Zheng Y. Removal of lead, copper, nickel, cobalt, and zinc from water by a cancrinite-type zeolite synthesized from fly ash. *Chemical Engineering Journal*. 1/1/ 2009;145(3):483-488.
43. Liu R, Liang P. Determination of trace lead in water samples by graphite furnace atomic absorption spectrometry after preconcentration with nanometer titanium dioxide immobilized on silica gel. *Journal of hazardous materials*. 2008;152(1):166-171.

\*\*\*\*\*